

Articulate That Object Part (ATOP): 3D Part Articulation from Text and Motion Personalization

ADITYA VORA, Simon Fraser University, Canada
 SAURADIP NAG, Simon Fraser University, Canada
 HAO ZHANG, Simon Fraser University, Canada



Fig. 1. Given a segmented (part highlighted) and textured mesh in rest state (left) in the input, we first generate multi-view videos (middle) of plausible part articulation using our personalized diffusion model. Using these multi-view videos we then transfer the motion back to 3D mesh (right). The meshes shown are the top retrieval results from Objaverse [Deitke et al. 2024] for the text queries: "Trashcan", "Cabinet", "Lamp".

We present ATOP (Articulate That Object Part), a novel method based on *motion personalization* to articulate a 3D object with respect to a part and its motion as prescribed in a text prompt. Specifically, the text input allows us to tap into the power of modern-day video diffusion to generate plausible motion samples for the right object category and part. In turn, the input 3D object provides *image prompting* to personalize the generated video to *that* very object we wish to articulate. Our method starts with a *few-shot finetuning* for category-specific motion generation, a key first step to compensate for the lack of articulation awareness by current video diffusion models. For this, we finetune a pre-trained multi-view image generation model for controllable multi-view video generation, using a small collection of video samples obtained for the target object category. This is followed by motion video personalization that is realized by multi-view rendered images

of the target 3D object. At last, we transfer the personalized video motion to the target 3D object via differentiable rendering to optimize part motion parameters by a score distillation sampling loss. We show that our method is capable of generating realistic motion videos and predict 3D motion parameters in a more accurate and generalizable way, compared to prior works.

1 INTRODUCTION

Everyday objects in the 3D world we live in undergo various movements and articulations. How the different parts of a 3D object move and interact with each other reflects the object's intended functions. As such, the ability to model and reason about object articulations in 3D plays an important role in simulation, design, autonomous systems, as well as robotic vision and manipulation. Over the past ten years, there has been a steady build-up of digital

Authors' addresses: Aditya Vora, Simon Fraser University, Canada; Sauradip Nag, Simon Fraser University, Canada; Hao Zhang, Simon Fraser University, Canada.

3D assets, from ShapeNet [Chang et al. 2015] (3M models) in the early days, to efforts on improving the assets’ structure (e.g., Part-Net [Mo et al. 2019] with 27K finely segmented models) and quality (e.g., Amazon Berkeley Objects (ABO) [Collins et al. 2022] with ~8K models), and to the latest and largest open-source repository Objaverse-XL [Deitke et al. 2023] (10M+ models). However, very few, if any, of these models come with part motions. Predominantly, they were all constructed in their rest (i.e., unarticulated) states. To our knowledge, the largest 3D datasets with part articulations, SAPIEN [Xiang et al. 2020] and Shape2Motion [Wang et al. 2019], only contain 2,346 and 2,440 *manually* annotated synthetic models, respectively. Clearly, human annotations are expensive in terms of time, cost, and expertise – they not scalable to endow large volumes of 3D assets with articulations and functions.

In this paper, we are interested in developing a learning method to generate *plausible* and *accurate* articulations for *any* given 3D object, *without* relying on any human-annotated 3D part motions as most existing methods [Abbatematteo et al. 2019; Hu et al. 2017; Jain et al. 2021; Mo et al. 2021; Wang et al. 2019] do. With the recent success of large foundation models, especially those built on diffusion [Yang et al. 2023], it is natural to leverage the zero shot and open vocabulary capabilities of the emerging *video diffusion models* [Blattmann et al. 2023a; Guo et al. 2023; Ho et al. 2022; Wang et al. 2024b; Xing et al. 2024] to first generate motion videos for our target object and then perform a 2D-to-3D motion transfer. This approach is (3D) annotation-free, hence more scalable, but faces three key challenges to obtain accurate 3D part articulations:

- First, SOTA video diffusion models [Blattmann et al. 2023a; Guo et al. 2023; Wang et al. 2023; Xing et al. 2024] are not yet well trained or sufficiently adaptive to generating articulations of everyday objects (e.g., even something as simple as a laptop), especially when typical *piecewise rigidity* is expected; see Fig. 2.
- Second, while current text-to-video models are capable of generating plausible motions for *some* object referenced in text prompt, to our knowledge, none of these methods can ensure that the generated motion is exactly of a *specific* (the target) *3D object*.
- Third, while current diffusion models, particularly multi-view video diffusion models, generate plausible motion, they lack fine-grained control over which specific part should move.

To address these challenges, we present a novel method based on *motion personalization* to articulate a 3D object in the form of a segmented mesh, with respect to a part prescribed in a text prompt. Specifically, the text input allows us to tap into the power of modern-day video diffusion models to generate plausible motion samples for the right object category and part. The input 3D object provides *image prompting* to personalize the generated video to *that* very object we wish to articulate. Our method is coined ATOP, for Articulate That Object Part, and it consists of three main steps:

- (1) *Finetuning for category-specific motion video generation.* This is a key first step to compensate for the lack of articulation awareness by current video diffusion models. We finetune a pre-trained multi-view *image* generation model, ImageDream [Wang and Shi 2023], for *controllable multi-view video* generation, using *few-shot* video samples obtained for the target object category, that are of different objects from the target object. We start

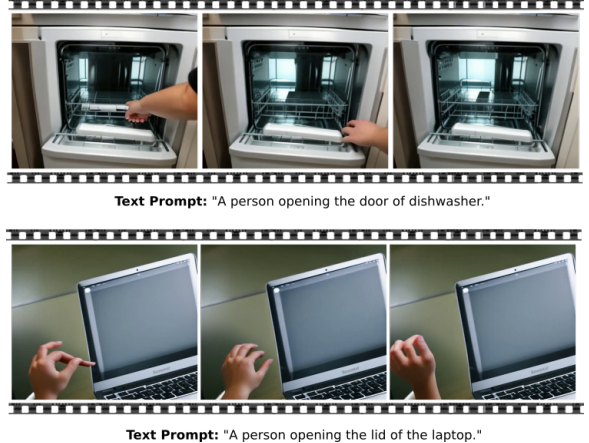


Fig. 2. When prompted to generate object articulations, Stable Video Diffusion [Blattmann et al. 2023a], a SOTA video diffusion model, cannot produce the desired part motion at all; only hand motions were observed.

from the pre-trained weights of ImageDream and inflate them for multi-view video processing. We opt to expand an image diffusion model for video generation due to its relatively higher articulation awareness, as demonstrated in Fig. 3. In addition, the signal for controlling part motion (i.e., the specific part we aim to articulate) is established using mask conditioning derived from a segmented mesh.

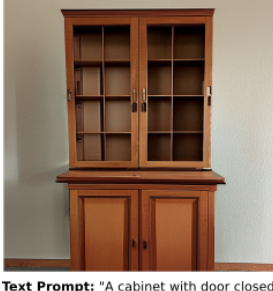
- (2) *Motion video personalization.* We render multi-view images and masks of the part which is to be articulated, for the target 3D mesh. These images, rendered masks, camera poses, and text prompt embeddings are fed to our finetuned video diffusion model, which *hallucinates* the desired part motion from multiple views, personalized to the target object.
- (3) *Video-to-mesh motion transfer.* Using the personalized output from the finetuned diffusion model, we transfer the video motion to the target 3D object via differentiable rendering, which optimizes the motion parameters associated with the prescribed part by a score distillation sample (SDS) loss [Poole et al. 2022]. In our current work, we only consider piecewise rigid part motions: revolute or prismatic.

An overview of our method is shown in Fig. 4. To our knowledge, ATOP presents the first annotation-free learning framework for generating accurate part articulations of existing 3D objects from text prompts. We present both qualitative and quantitative experiments to demonstrate that our method is not only capable of generating realistic personalized motion videos on unseen shapes, but also transferring the motion to 3D meshes, resulting in more accurate articulations in 3D than prior works.

2 RELATED WORK

2.1 Mobility Analysis of Shapes

Feedforward articulation. Understanding part mobility is crucial for object kinematics [Abbatematteo et al. 2019; Mo et al. 2021]. Recent data-driven approaches leverage increasing 3D data and articulation annotations. ScrewNet [Jain et al. 2021] predicts articulation



Text Prompt: "A cabinet with door closed"



Text Prompt: "A cabinet with door open"

Fig. 3. Samples generated from a Text to Image diffusion model [Rombach et al. 2022a]. As can be seen, unlike video diffusion model (Fig. 2) image diffusion models have relatively higher articulation awareness which eases the finetuning process.

from depth image sequences without part segmentation, while Hu et al. [Hu et al. 2017] estimate mobilities by mapping point clouds to motion classes. However, part segmentation often fails to align with part mobilities. To address this, Shape2Motion [Wang et al. 2019] jointly computes motion-oriented segmentation and attributes from a single point cloud, trained with extensive manual annotations. Yet, limited annotated data hampers the generalization ability of the model. Self-supervised methods [Liu et al. 2023a; Wei et al. 2022] reconstruct object surfaces using neural radiance fields, requiring multiple articulation states. While these methods generalize well, they are challenging to scale due to their high input requirements and dependence on articulated inputs, which are not available for static meshes. In contrast to these self-supervised methods, we aim to learn articulation for a 3D object category from few-shot video samples using foundation models like video diffusion, and then generalize to category specific new target meshes.

Generative articulation. With the rapid advancements in generative AI in recent years, the task of learning to represent, reconstruct, and generate object articulations from various input sources has become a prominent research area in visual computing [Le et al. 2024; Li et al. 2024; Uzolas et al. 2024]. NAP [Lei et al. 2023] employed diffusion models to synthesize articulated 3D objects by introducing a novel articulation graph parameterization. However, it faced limitations in scalability and controllability for articulations. CAGE [Liu et al. 2024b] addressed these challenges by jointly modeling object parts and their motions within a graph-based structure. Recently, [Liu et al. 2024a] proposed the seminal task of generating articulated objects from a single image. In contrast to these existing approaches that are focused on generating articulated assets, our goal is to enhance existing 3D assets by incorporating precise articulations.

2.2 Motion Personalization

Diffusion models [Ho et al. 2020; Song et al. 2020a,b] have garnered significant interest for their training stability and remarkable performance in text-to-image (T2I) generation [Balaji et al. 2022; Ramesh et al. 2021]. Video generation [Le Moing et al. 2021; Luo et al. 2023; Yu et al. 2023a] extends image generation to sequential frames, incorporating temporal dynamics. Recent advancements [Alimohammadi et al. 2024; Ge et al. 2023; Nag et al. 2023; Singer et al. 2022a;

Zhou et al. 2022] adapt T2I diffusion models to spatio-temporal domains via architectural modifications. Personalizing motion using reference videos has gained traction, with methods like Tune-a-Video [Wu et al. 2022] enabling one-shot video editing with structural control. Current approaches [Jeong et al. 2023; Materzynska et al. 2023] refine pre-trained text-to-video (T2V) models using regularization or frame residual losses, reducing dependency on training video appearances. Subject-driven video generation [Molad et al. 2023; Wu et al. 2023; Zhao et al. 2024] fine-tunes video diffusion models but often struggles with overfitting and limited motion dynamics, failing to accurately capture 3D articulations. In contrast, our method leverages multi-view videos to customize motion, enabling precise transfer to 3D articulated objects.

2.3 Text to 3D Motion

Dreamfusion [Tang 2022] introduced the score distillation framework for text-to-3D shape generation. Such per-object optimization methods have also been extended to the dynamic 3D domain [Singer et al. 2023] where they leverage video diffusion models [Blattmann et al. 2023b; Singer et al. 2022b]. Some methods [Uzolas et al. 2024] combine the guidance from video diffusion models with multiview [Shi et al. 2023] and single-image diffusion models [Rombach et al. 2022a] to boost 3D consistency and individual frame quality [Zheng et al. 2024], and they utilize different forms of score distillation [Wang et al. 2024a; Yu et al. 2023b]. By utilizing image conditional diffusion priors such as Zero123 [Liu et al. 2023b] and ImageDream [Wang and Shi 2023] as guidance, this approach has also been applied to the video-conditional 4D generation setting by Consistent4D [Jiang et al. 2023] and DreamGaussian4D [Ren et al. 2023].

3 PRELIMINARIES

Multiview Image Diffusion Model. Latent Diffusion Models (LDMs) are generative models that learn the data distribution by compressing it into the latent space of an autoencoder and then applying a UNet [Ho et al. 2020; Sohl-Dickstein et al. 2015; Song and Ermon 2019] within this space. Multiview Image Diffusion Models like MV-Dream [Shi et al. 2023] and ImageDream [Wang and Shi 2023] fall into a category of diffusion models that are explicitly trained for multi-view image generation. The core of these models is powered by correspondence-aware 3D self-attention, which aids the overall 3D consistent generation. For our task, where we require correspondence across multiple views along-with temporal consistency, we piggyback on the pre-trained weights of one such diffusion model ImageDream. The main advantage of using this model is to have an additional modality for controlling the generation in the form of *image conditioning*, which offers significant advantages compared to methods which solely rely on text prompts for generation. These models generally generate 3D in two stages. In the first stage, multi-view diffusion model is trained to generate consistent multi-view images from a text-prompt and single image conditioned on the respective camera embedding. In the second stage, the 3D model is reconstructed using the generated images with a NeRF-like [Mildenhall et al. 2021] representation. Formally, given an input set $\mathcal{I} = \{z_{mv}, f_{txt}, f_{img}, c_{mv}\}$ during training, where z_{mv} is the latent embedding of multi-view input images extracted from VAE [Kingma

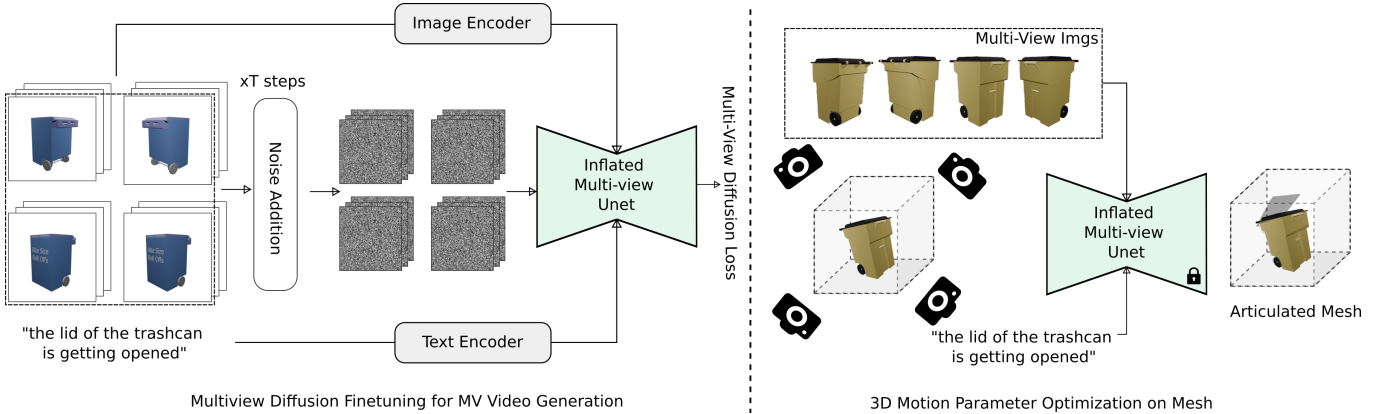


Fig. 4. Pipeline Overview: Given a small collection of multi-view videos belonging to the same category our goal is to learn a category specific motion by finetuning a multi-view image diffusion model. For this, noise is added to the latents of the multi-view videos and then denoised using the UNet blocks. Appearance information is injected into the UNet using cross attention between first frame of multi-views and the latents, using a CLIP [Miller et al. 2020] image encoder. Once finetuned, we can adapt the model for a new mesh and optimize the motion parameters with score distillation loss using the guidance from personalized diffusion model.

and Welling 2013a], f_{txt} and f_{img} are the text-prompt and image embeddings, whereas c_{mv} are the camera embeddings. This DM is then optimized using multi-view diffusion loss as,

$$\mathcal{L}_{LDM} = \mathbb{E}_{z_{mv}, f_{txt}, f_{img}, c_{mv}, \epsilon, t} [\|\epsilon - \epsilon_\theta(z_t; f_{txt}, f_{img}, t, c_{mv})\|^2]. \quad (1)$$

We adopt ImageDream as our base multi-view model for the following reasons: (1) To leverage the 3D correspondence-aware self-attention for multi-view consistent generation. (2) Because ImageDream is an Single Image-to-Multi-View model, we can adapt it for generating *personalized* motion based on the input images of a static 3D mesh given during inference.

Inflated UNet. A Text2Image (T2I) diffusion model, such as LDM [Rombach et al. 2022b], typically adopts a U-Net architecture [Ronneberger et al. 2015], which comprises of a downsampling phase followed by upsampling with skip connections. This architecture is structured using stacked 2D convolutional residual blocks, spatial attention blocks, and cross-attention blocks that integrate embeddings derived from textual prompts. To adapt the T2I model for Text2Video (T2V) tasks, the convolutional residual blocks and spatial attention blocks are modified through inflation. Consistent with prior work [Cong et al. 2024; Wu et al. 2022], the 3×3 convolution kernels in the residual blocks are replaced with $1 \times 3 \times 3$ kernels by introducing a pseudo-temporal channel. To improve temporal coherence, the spatial self-attention mechanism is also extended to the spatio-temporal domain. While the original spatial self-attention mechanism operated on patches within individual frames, the inflated U-Net leverages patch embeddings across the entire video as queries, keys, and values. This design facilitates a comprehensive understanding of the video context. Furthermore, the parameters from the original spatial attention blocks are reused in the newly designed dense spatio-temporal attention blocks.

Score Distillation Sampling. It is a method that enables using a diffusion model as a critic, i.e., using it as a loss without explicitly back-propagating through the diffusion process. To perform score distillation, noise is first added to a given image (e.g., one novel

view). Then, the diffusion model is used to predict the added noise from the noised image. Finally, the difference between the predicted and added noises is used for calculating per-pixel gradients. The per-pixel score distillation gradients is given as:

$$\nabla_\theta \mathcal{L}_{SDS}(\mathbf{z}, \tau, \epsilon, t) = \mathbb{E}_{t, \epsilon} \left[\omega(t) (\epsilon_\phi(z_t; t, \tau) - \epsilon) \frac{\partial \mathbf{z}_t}{\partial \theta} \right] \quad (2)$$

where θ represents the parameters of the 3D representation, \mathbf{z} is the rendered latent at the current view, τ is the text prompt, t is the timestamp in the diffusion process, ϵ the ground truth noise, ϵ_ϕ is the UNet with frozen parameters ϕ , whereas \mathbf{z}_t is the latent obtained by adding noise in timestep, t . During training, the gradients flows from the pixel gradients to the 3D representation.

4 METHOD

In the following subsections, we first describe the problem setting in Sec. 4.1. In Sec. 4.2 we describe our finetuning step for multi-view video generation. In Sec. 4.3 we describe the motion personalization step and finally in Sec. 4.4 we explain the 3D motion inference step. And finally in Sec. 4.5 we brief about losses used to train the model.

4.1 Problem Setting

Given a small collection \mathcal{V} of multi-view (4 views) videos of a few (8) articulated objects belonging to the same category (e.g., trashcans), along with a motion prompt τ (e.g., “The lid of the trash can is getting opened.”), our goal is to learn category-specific and part-aware motion pattern and adapt them to a novel, target 3D mesh \mathcal{M} from the same category. To simplify learning and enhance generalization to new shapes, we propose training a separate diffusion model for each motion type. For example, we train distinct models for cabinet doors opening to the left and right. By decomposing complex motions into simpler patterns, this approach makes motion learning more efficient and improves generalization, even with limited training data. Given this small video collection, it serves as few-shot training samples for our finetuning step, where these

videos are of articulated objects different from the target object. It is possible for these objects to all exhibit structural and/or topological differences, as long as they belong to the same category. In addition, to inject control signal over part motion, we also take a binary mask of the *first frame*, of the part which we want to articulate. This mask, during inference step, can be rendered from a segmented mesh.

Overview. To address this challenge, we decompose the problem into two main stages: *a) Motion Personalization* and *b) 3D Motion Transfer*. In the first stage, the multi-view videos \mathcal{V} and the motion prompt τ are utilized to capture the motion dynamics of the object’s parts. This is achieved by fine-tuning a pretrained image-to-multi-view diffusion (I2MV) model [Wang and Shi 2023], enabling the synthesis of multi-view video data. In the second stage, the synthesized multi-view videos are employed to extract the motion axis within 3D space, which subsequently guides the articulation of the 3D mesh \mathcal{M} . An overview of the problem formulation and the proposed methodology is depicted in Fig. 4.

4.2 Finetuning Multi-View Video Diffusion Model

Prior works [Liu et al. 2023a] have shown the possibility of recovering the motion parameters from *multi-view* images of different articulation states using a NeRF representation. However, given a *static* mesh in the *rest state*, it is impossible to have such multi-view articulated input conditions for recovering the motion parameters. Hence, we propose an approach where we first *generate* multi-view videos of part articulation for the target object. These multi-view videos provide a more reliable basis for estimating the motion axis in 3D space, leading to the desired articulation of the 3D mesh. Since, current SOTA diffusion models lack articulation priors as shown in Fig. 2, we propose a finetuning step, where we first inflate a multi-view image DM for multi-view video generation.

Correspondence aware spatial attention. We build our multi-view video diffusion model on the pre-trained 3D-aware diffusion model, ImageDream [Wang and Shi 2023]. While ImageDream’s spatial modules ensure geometric consistency across views, they are not designed for temporal processing. To address this, we inflate these layers (Sec. 3) to enforce geometric consistency across views at each frame index. Let $V \in \mathbb{R}^{B \times N_v \times N_f \times F \times H_1 \times W_1}$ denote the 6D feature tensor of a multi-view video in the diffusion model, where B , N_v , N_f , F , H_1 and W_1 are batch size, number of views, number of frames, channel dimension, height and width of the video respectively. We first encode these video frames to latents Z using VAE encoder \mathcal{E} [Kingma and Welling 2013b] after reshaping the tensor to size $(B N_v N_f) \times F \times H_1 \times W_1$. The VAE resizes the tensor to resolution H and W . The tensor is then passed through the ResNet block after reshaping the tensor to support temporal processing as explained in Sec. 3. Post the ResNet layer, we pass the tensors through the self-attention block before which we concatenate the tensors across all frames and views into tokens which results in a tensor of size $(B N_v N_f) \times (H W) \times F$. Post this, self-attention is applied across all views which is given as:

$$Z_{\text{out}} = \text{reshape}(Z, (B N_v N_f) (H W) F \rightarrow (B N_f) (N_v H W) F) \quad (3)$$

Here, Z_{out} is the output tensor after reshaping operation which becomes Z for next layers. Unlike regular inflation in stable diffusion

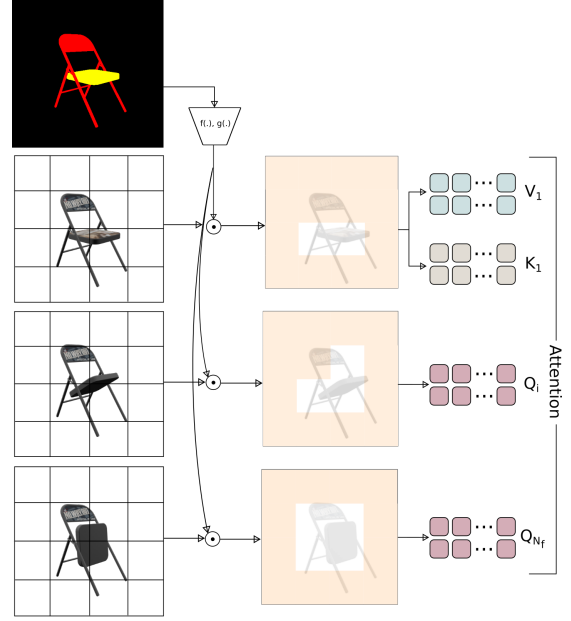


Fig. 5. Temporal Attention Block. We modulate latent using the affine transformation where the transformation is predicted by the blocks $f(\cdot)$ and $g(\cdot)$. Post this step, attention is applied between the 1^{st} and n^{th} frame.

models [Wu et al. 2022] where the self-attention block is inflated for temporal processing, here, in multi-view diffusion models, the self-attention blocks are 3D correspondence aware and hence is more suitable for geometric consistency across views rather than temporal consistency. We model the temporal consistency using a temporal block as explained in next section.

Camera Controllability. MV DM is controllable by camera poses by incorporating a camera pose sequence as input. These poses are first encoded using MLP layers, after which the resulting embeddings are combined with the timestep embeddings. The combined embeddings are subsequently fed into the attention block of the UNet by adding these embeddings to the latent obtained from the ResBlocks.

Cross Attention for Appearance Injection. To ensure consistency in object appearances across varying viewpoints or motion, we integrate appearance information into the diffusion model. This enables the model to preserve consistent visual features, such as textures, colors, and details, across multiple views and frames, enhancing both the realism and coherence of the generated outputs, particularly in dynamic scenes. To achieve this, *multiple views (e.g., 4) of the object’s rest state* are fed into the cross-attention block of the UNet. This allows the diffusion model to utilize contextual information during generation within a text-aligned embedding space. Specifically, we employ a pre-trained CLIP image encoder to embed the multi-view images into a latent space represented by Z , and subsequently fuse them as follows: 1) For attention between the text and image tokens we first reshape the latents as below:

$$Z_{\text{out}} = \text{reshape}(Z, (B N_f) (N_v H W) F \rightarrow (B N_f N_v) (H W) F) \quad (4)$$

Note that, rather than a single image we have multi-view images of starting frames of video. To effectively inject the appearance information of each view into the respective latents, we repeat the

image tokens of each view to all frames of the respective view and then use this tokens for cross attention. Next, the text and image tokens are fused together via:

$$F_{\text{out}} = \text{Attention}(Q, K_{\text{txt}}, V_{\text{txt}}) + \lambda \cdot \text{Attention}(Q, K_{\text{img}}, V_{\text{img}}) \quad (5)$$

Here, Q represents the query tokens derived from the latent Z_{out} in Eq. 4, keys and values for the text embeddings are K_{txt} and V_{txt} , while K_{img} and V_{img} represent keys and values of image tokens.

Spatio-Temporal Module. Besides spatial 3D consistency which is attained by the pre-trained correspondence aware self-attention blocks, it is crucial for multi-view video diffusion models to maintain the temporal coherence of generated multi-view videos simultaneously. In order to process the temporal information in the video, we add an additional sparse temporal attention block which interpolates the temporal features between the first frame and the n^{th} frame of the video via attention. Inspired from [Perez et al. 2018] to control the motion output of the diffusion model based on the part we want to articulate, we adaptively influence the output of the model by applying an affine transformation to the network’s intermediate features based on the mask input (denoted by \mathcal{B}). We map the mask input using functions $f(\cdot)$ and $g(\cdot)$ which output γ and β which are then used to modulate the latents as $Z_{\text{out}} = \gamma \odot Z + \beta$. We use 2 layer convolutional blocks for mapping functions $f(\cdot)$ and $g(\cdot)$. A brief overview of our temporal attention block is shown in Fig. 5. To apply attention we reshape the latent as follows:

$$Z_{\text{out}} = \text{reshape}(Z, (B N_f N_v) (H W) F \rightarrow ((B N_v H W) N_f F) \quad (6)$$

We then take attention between the first and last frame as,

$$Z_{\text{out}} = \text{Attention}(Q_i, K_1, V_1) \quad (7)$$

Where, Q_i are the query tokens of i^{th} frame, whereas K_1 and V_1 are the keys and values of the first frame. This final Z_{out} is passed into the decoder VAE to obtain multi-view video output.

4.3 Personalized Motion Generation.

Post finetuning step we obtain a multi-view video diffusion model, ψ^* , which can hallucinate the motion of a particular part of the target mesh from different views. In order to generate personalized motion for a mesh, we first render the target 3D mesh in its rest state, into multi-view images from the fixed camera poses used during finetuning. Post that, using the text prompt (τ) and multi-view images, \mathcal{I}_r we infer the motion from different views for the input object. It is obtained as follows:

$$\hat{\mathcal{V}} = \psi^*(\mathcal{I}_r, \tau, \mathcal{B}) \quad (8)$$

where \mathcal{I}_r is the rendered image of the target mesh and \mathcal{B} is the part segmentation mask rendered using the segmented mesh respectively. This personalized multi-view motion $\hat{\mathcal{V}}$ is further used to estimate the 3D articulation of the target mesh.

4.4 3D Motion Inference

Post the personalization step, we transfer the motion generated by our diffusion model back to 3D from multiple views using a differentiable rendering approach which is optimized using a score distillation loss [Poole et al. 2022]. We represent the geometry of the input shape using a mesh \mathcal{M} , defined by a set of vertices $\mathcal{V} \in \mathbb{R}^{n \times 3}$

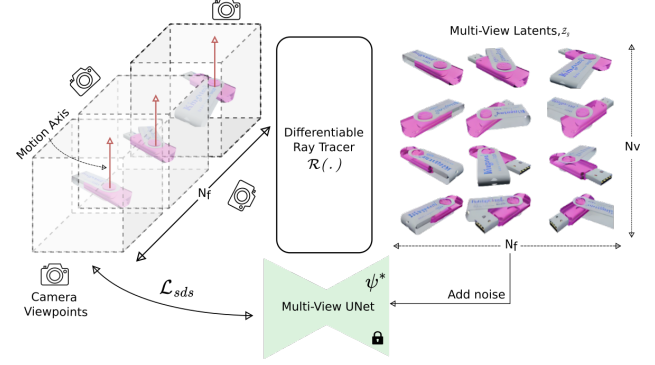


Fig. 6. Approach for 3D motion transfer. We render the multi-view latent \mathcal{Z}_g using our differentiable renderer $\mathcal{R}(\cdot)$ and then optimize these latent using the guidance from our personalized motion model ψ^* .

and faces $\mathcal{F} \in \{1, 2, \dots, n\}^{m \times 3}$. In order to estimate the motion parameters, we first optimize for coarse articulation states in the 3D space using the guidance from our personalized diffusion model (Eq. 8) respectively. For this, we parameterize each video frame for timestep $t = \{t_1, t_2, \dots, t_{N_f}\}$ using a set of N_g gaussians. Each gaussian is represented with a center $\mu \in \mathbb{R}^3$, covariance $\Sigma \in \mathbb{R}^{3 \times 3}$, weights $\lambda \in \mathbb{R}$ and features $f_g \in \mathbb{R}^4$, which are learnable parameters. Using these parameters, multivariate gaussian, $G(\cdot)$ is defined as:

$$G(\vec{x}) = |\Sigma|^{\frac{-1}{2}} \exp^{\frac{-1}{2}}(\vec{x} - \mu)^T \Sigma^{-1}(\vec{x} - \mu) \quad (9)$$

where, \vec{x} is a point in 3D space, $\vec{x} \in \mathbb{R}^3$. Given these gaussians, we choose to optimize their locations in the *latent space* of the diffusion model [Metzler et al. 2023]. For this, the distance of i^{th} gaussian to ray \vec{v} is given as (applying log to Eq. 9):

$$d(\vec{v}t_i) = \frac{-1}{2} [(\vec{v}t_i - \mu)^T \Sigma^{-1}(\vec{v}t_i - \mu)] + \log(\lambda_i) \quad (10)$$

where, $\vec{v}t$ is the gaussian intersection with ray \vec{v} . The intersection t_i for i^{th} gaussian is computed as $t_i = \frac{\mu_i^T \Sigma^{-1} v}{v^T \Sigma^{-1} v}$. Given this distance function the blending weights for each ray is computed as:

$$w_i = \exp(\beta_1 d_i - \frac{\beta_2}{\eta} t_i) \quad (11)$$

here, w_i , d_i and t_i represent weights, distance and intersection of i^{th} gaussian respectively. Whereas β_1 , β_2 and η are hyperparameters. After computing the blending weights for each ray using Eq. 11 we render features for each frame by blending the features of each gaussian as per the blending weights. $\mathcal{Z}_g = \frac{1}{\sum_i w_i} \sum_i w_i f_{g_i}$. Having rendered all the frames from multiple views using the renderer, we then optimize this renderer $\mathcal{R}(\cdot)$ to generate most plausible multi-view videos with the help of guidance from *frozen* multi-view diffusion model (ψ^*). By optimizing in the above step, we get a sparse point cloud of an articulated shape for frame at each time step. However, our final goal is to estimate the motion hyperparameters i.e. *motion axis* and *motion origin*. In our current work we only consider piecewise rigid motions like *revolute* and *prismatic*. Having known the static mesh \mathcal{M} we sample points on the segmented part which we want to articulate and approximate it using an oriented bounding box (OBB). Based on the parameters of the OBB we select

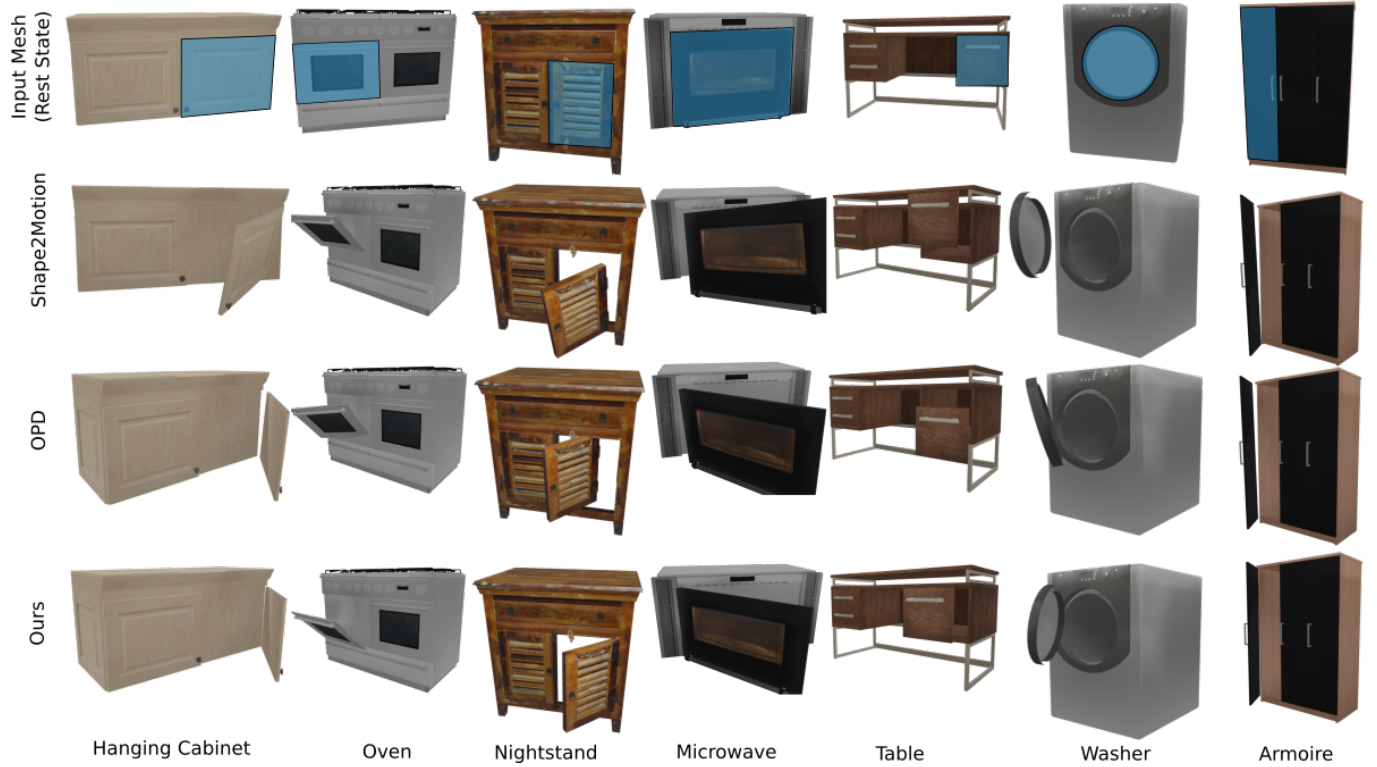


Fig. 7. Qualitative results of part articulation on ACD dataset [Iliash et al. 2024] The part which is to be articulated is highlighted in the first row. Note: The models in ACD dataset does not have interiors.

7 possible axis origins and 6 possible axis directions. These possible axis origins are obtained by computing centers of each side face of the OBB plus one centroid. Whereas, the possible axis directions are the 3 principal components of the OBB. The other 3 are obtained by negating the original principal components of the oriented bounding box. We then transform the set of points representing the dynamic part (desired part to articulate) using piece-wise rigid assumption. We then select the best axis and origin as the one which minimizes the chamfer distance with the articulated point cloud. For more details, read the supplementary.

4.5 Training Objectives

We train our model in a two stage paradigm: (a) Motion Finetuning and (b) 3D Transfer respectively.

Finetuning Stage. In our finetuning step, we freeze the entire DM and just train the temporal attention block (Eq. 7). In addition to this we also update the weights of the query projection layers of self and cross attention blocks. During this stage the network is optimized using multi-view diffusion objective \mathcal{L}_{LDM} as mentioned in Eq. 1. *3D Motion Transfer Stage.* During the 3D motion inference stage we optimize the gaussians with SDS loss as mentioned in Eq. 12. However, because we condition our generation on multi-view images \mathcal{I}_r and masks \mathcal{B} the loss is defined as:

$$\nabla_{\theta} \mathcal{L}_{SDS} = \mathbb{E}_{t, \epsilon} \left[\omega(t) (\epsilon_{\phi}(z_{g_t}; t, \tau, \mathcal{I}_r, \mathcal{B}) - \epsilon) \frac{\partial z_{g_t}}{\partial \theta} \right] \quad (12)$$

where, θ are the parameters of the differentiable renderer $\mathcal{R}(\cdot)$, ϵ_{ϕ} is the UNet from the personalized diffusion model, ψ^* . z_{g_t} is the latent rendered from the renderer added with noise for timestep, t . τ , \mathcal{I}_r and \mathcal{B} is the text-prompt, rendered image from the target mesh and segmentation mask respectively.

5 EXPERIMENTS

In this section, we present the qualitative and quantitative results of our method’s ability to infer 3D motion parameters given only a static segmented mesh as input. Along with it we also compare our multi-view video outputs with other baselines.

5.1 Dataset and Metrics

Dataset details. For a comprehensive quantitative and qualitative assessment of our approach, we utilize data from the PartNet-Mobility dataset [Xiang et al. 2020] to finetune our diffusion model. Based on the number of shapes within a category we create train and test splits for PartNet-Mobility dataset. On an average we select 8 objects for finetuning our diffusion model and keep the remaining shapes within the category for testing i.e. 3D motion inference. For each shape available for training we render 4 view videos per shape showcasing an articulation. For e.g. the seat of a folding chair getting folded. While the video is captured, we assume that the 3D mesh is scaled to unit sphere. We capture the videos at orthogonal viewpoints where each azimuth angle is set to $[45^\circ, 135^\circ, 225^\circ, 315^\circ]$

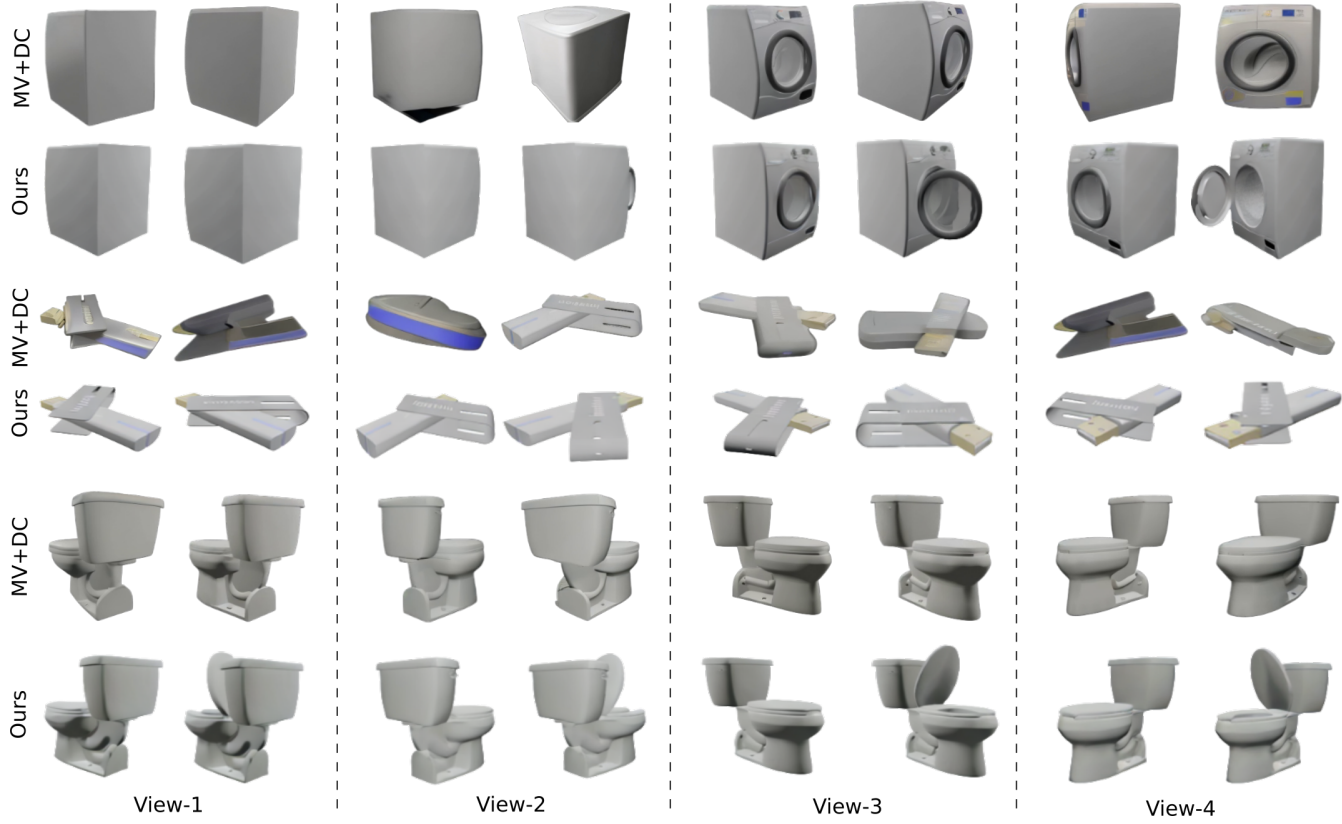


Fig. 8. Qualitative comparison results of multiview video generation.

respectively. The elevation is set to 10° for some categories whereas 30° for others. For each view, we capture 10 frames of 512×512 resolution. However, since ImageDream aspects 256×256 resolution input we scale the videos to that resolution during finetuning. In addition to RGB input, as described previously we also take binary masks of the first frame of the part which we want to articulate from multiple views as input, for this, we render the mask from the same camera viewpoints with a colored mesh with part labels. Furthermore, to evaluate the model’s generalization capabilities, we conduct *zero-shot* experiments using 135 objects from the ACD dataset [Iliash et al. 2024] which is composed of challenging objects from ABO [Collins et al. 2022], 3D-Future [Fu et al. 2021] and HSSD [Khanna et al. 2024] datasets. This dataset already has textured segmented meshes with its part annotations. For testing the generalization capabilities of the model, we render multi-view images along with the segmentation mask from multi-views similar to PartNet mobility. Here, the camera viewpoints are also the same as used in PartNet mobility and the mesh is scaled to unit sphere. This split is the same as the one curated by [Liu et al. 2024a].

Metrics Details. We evaluate our approach through a two-step comparison with baselines for multi-view video generation and 3D motion parameter estimation. For temporal coherence, we compute Frechet Video Distance (FVD) [Unterthiner et al. 2019]. To assess text alignment, we measure the CLIP score [Miller et al. 2020]. Spatial and

temporal consistency are quantified using PSNR and LPIPS [Zhang et al. 2018]. Additionally, we evaluate 3D motion transfer quality using standard metrics from [Jiang et al. 2022; Wang et al. 2019]: Mean Angular Error (MAE) and Mean Position Error (MPE). MAE is computed as the dot product similarity between the predicted and ground truth motion axes, while MPE measures the Euclidean distance between the predicted and ground truth joint origins.

Implementation details. Our implementation is based on the Pytorch framework [Paszke et al. 2019]. For diffusion, we use a popular library diffusers [von Platen et al. 2022]. In both stages i.e. during finetuning as well as during 3D motion transfer stage we use Adam optimizer [Kingma and Ba 2014] to update the trainable parameters. During the finetuning stage, we set a learning rate of $5e^{-4}$, whereas during the 3D motion transfer stage, we set a learning rate of $5e^{-3}$. As stated before, we train separate models for each motion pattern within a category. For example, in the storage category, distinct models are learned for the motion of left doors, right doors, and drawers. During finetuning, we train the model for 20000 iterations. A single multi-view video sample comprises of 4 views and 10 frames each. The resolution of each video is 256×256 . During the personalization step, we do inference for 50 steps using a classifier-free guidance scale of 5.0. Both finetuning and inference are done with fp16 model weights of ImageDream. During inference, we render the image using Blender, whereas the masks are



Text Prompt: "The door on the left side of the storage furniture is getting opened."

Text Prompt: "The door on the right side of the storage furniture is getting opened."

Text Prompt: "The drawer of the storagefurniture is getting opened."

Fig. 9. Effect of Masking in Articulation. Our multi-view diffusion model enables controllable motion generation through masking. By applying a mask, we can selectively control where articulation occurs, allowing for plausible motion generation at any specified location.

rendered using Pytorch3D [Ravi et al. 2020]. We finetune a single personalized diffusion model on Nvidia V100 GPU with 32Gb GPU memory. The training takes approximately 5hrs to complete. During inference, we sample 2048 points each on both static and dynamic part of the mesh and then initialize the gaussian centers with it. For our renderer, we set $\beta_1 = 21.4$, $\beta_2 = 2.66$. Because we optimize the points within the latent space of the diffusion model [Metzger et al. 2023], we render features of resolution 32×32 .

5.2 Baselines & Result Discussions

To the best of our knowledge, this work is the first to address the problem of 3D mesh articulation through motion personalization. Consequently, no prior baseline directly utilizes the same input format or produces the same output as our approach. Instead, we assess individual components of our pipeline by benchmarking them against appropriate baselines tailored to each step.

Multi-View Video Generation Baselines. Since there are no previous works which directly predict multi-view videos from *static multi-view images* we create baselines for this task. First baseline is based on dynamicrafter [Xing et al. 2024] where multi-view (MV) images of the target mesh is provided as input to the pre-trained video diffusion model to generate videos from multiple views in a zero-shot manner. For this baseline we perform a direct inference using the pre-trained weights of DynamiCrafter[Xing et al. 2024](DC). We denote this baseline as MV+DC respectively. For the second baseline, we finetune ImageDream model, without temporal attention in order to process videos directly. Except temporal attention all the layers which we train in our finetuning stage are trained for this baseline. We denote this baseline as ID[†] respectively.

3D Motion Parameter Estimation Baselines. For the 3D motion transfer stage, our pipeline takes a static, segmented 3D mesh as input and estimates the parameters of the 3D motion axis using the motion outputs generated by the multi-view diffusion model. To benchmark this step, we compare our method against Shape2Motion (S2M) [Wang et al. 2019] and Openable Part Detection (OPD) [Jiang et al. 2022]. Shape2Motion takes a point cloud as input and estimates the motion parameters as output. The model is trained end-to-end with 3D ground truth. We train the Shape2Motion model on PartNet-Sapien dataset with the same train split which we use to finetune our diffusion model. Once trained the model is than evaluated against the objects in the test split within the PartNetSapien dataset. Along-with Shape2Motion, we also compare our method with OPD [Jiang et al. 2022]. OPD is a method to estimate motion parameters in 3D space using a single image as input. It uses a object detector backbone which directly infers the segmentation mask, motion type and motion parameters as output. We retrain all these baselines using the same data used to finetune our diffusion model. For shape2motion we use an upgraded model architecture as proposed in [Iliash et al. 2024]. We emphasize on the fact that, all these models despite trained in a few shot setting require 3D ground truth whereas our model infers 3D motion parameters directly from multi-view videos hence eliminating the requirement of GT motion annotations.

For comparing the generalization of all these methods with ours, we directly infer motion parameters in a feed-forward manner for these baselines. As shown in Table 1, Table 2 and Fig. 7 our method can generate plausible motion parameters compared to state of the art despite not using 3D annotations. Shape2Motion as observed in Table 1 performs better than OPD. This is because Shape2Motion infers the 3D motion parameters from a point cloud which aids the

Table 1. Quantitative results of Motion Parameter Estimation on PartNet-Mobility Dataset [Xiang et al. 2020]

Metric	Method	Categories										Mean
		Dishwasher	Display	Chair	Microwave	Lamp	Oven	Fridge	Storage	Washer	Glasses	
Ang Err ↓	S2M	8.93	4.21	8.33	3.82	9.76	7.97	5.44	5.28	6.58	10.12	7.04
	OPD	10.65	13.83	11.52	15.37	17.27	11.45	12.27	6.32	9.34	13.53	12.15
	Ours	1.95	0.83	5.77	1.14	3.64	1.36	1.77	1.65	3.81	4.47	2.63
Pos Err ↓	S2M	0.12	0.11	0.29	0.07	0.22	0.05	0.04	0.14	0.12	0.08	0.12
	OPD	0.21	0.17	0.36	0.09	0.18	0.08	0.08	0.12	0.11	0.16	0.15
	Ours	0.18	0.16	0.28	0.03	0.13	0.03	0.03	0.17	0.04	0.05	0.11

Table 2. Quantitative evaluation of zero-shot generalization on ACD dataset [Iliash et al. 2024].

Metric	Method	Categories									Mean
		Armoire	Cabinet	NightStand	Table	Microwave	Oven	Refrigerator	Washer		
Ang Err ↓	S2M	17.32	19.34	22.37	21.62	23.56	22.56	25.42	19.77	21.49	
	OPD	12.37	9.26	10.62	8.43	16.46	14.93	13.62	11.21	12.11	
	Ours	2.83	3.29	3.92	2.39	3.52	3.34	2.96	6.75	3.63	
Pos Err ↓	S2M	0.15	0.22	0.19	0.16	0.16	0.13	0.15	0.15	0.17	
	OPD	0.22	0.25	0.19	0.21	0.25	0.27	0.19	0.18	0.22	
	Ours	0.06	0.07	0.54	0.19	0.12	0.09	0.11	0.04	0.16	

prediction in comparison to OPD which infers the motion parameters from an image. However, as observed in Table 2 the performance of Shape2Motion significantly falls when tested on the generalization dataset. This is due to the limited generalization ability of the 3D backbone network. In comparison to these approaches our method can generalize well. This is because of two main reasons: 1) Diffusion model is trained with large amount of data because of which it has strong generalization ability compared to feed forward networks trained from scratch. 2) We confine the motion learning to a single motion pattern i.e. we train separate personalized diffusion model for each motion hence increasing the generalizability with limited representation power which prevents over-fitting. Beyond 3D motion parameter estimation, we also compare our multi-view video generation results with the baselines. As shown in Table 3 and Fig. 8, our method outperforms the baselines in LPIPS, PSNR, and FVD, while achieving comparable CLIP scores. Fig. 8 highlights that MV+DC preserves the appearance of multi-view image inputs across all frames. However, it struggles with geometric consistency across views and has no articulation motion, reinforcing our claims in Sec. 1 and Fig. 2. In contrast to this, as can be seen in Fig. 8 and Table 3 our results achieves best PSNR, LPIPS and FVD scores which shows that our method is able to generate 3D consistent output along with successful articulation as a result of which we can transfer the motion output from multi-views back to 3D. Thanks to the 3D correspondence aware self-attention and temporal attention blocks of our personalized diffusion model. In addition, our method is also controllable using a binary mask using which we can articulate all the parts of interest for a particular shape by just changing the mask location. This can be seen in Fig. 9.

6 CONCLUSION, LIMITATION, AND FUTURE WORK

We have presented ATOP, a first method aimed at endowing *existing* 3D assets with plausible and accurate part articulation in a scalable

Method	CLIP (↑)	FVD (↓)	LPIPS (↓)	PSNR (↑)
MV + DC	25.51	1587.23	0.587	10.27
ID [†]	24.27	1258.37	0.373	13.79
Ours	24.89	963.92	0.132	20.06

Table 3. Quantitative evaluation of video generation

way, through text prompting and motion personalization. This effort should be distinguished from related works whose goal is to *generate* articulated motions, either from text prompts or sparse images, both involving 3D reconstruction — we do not. Since 3D reconstruction from sparse inputs is still far from solved and even the most advanced methods to date cannot produce results of adequate quality, we believe that our problem setting is more realistic and holds stronger potential to make a more immediate impact on enhancing the world of digital 3D assets.

Despite the overall high accuracy from the 3D part articulations obtained by ATOP, our method still has its limitations. The first is the inability to generate completely photorealistic outputs, and sometimes produces unexpected hallucinations, inaccurate part boundaries, moved parts that are not perspective accurate, and revealed interiors that's not realistic. While such videos are sufficient for 3D motion parameter estimation, as shown in the previous section, they are still not production ready if the goal is to directly display the generated videos. Furthermore, our method currently only supports limited type of motions, and struggles to handle more complex motions involving multiple parts at once, or motions containing non-rigid parts. However, our method can realibly handle any motion of the same type and can infer different part motion in different inference steps.

For future work, besides addressing the limitations above, we would like to continue improving the scalability of our approach in terms of object categories and the ability to support cross-category motion transfer, e.g., to open all the doors of vehicles, rooms, etc.,

with only few-shot training from video samples of opening cabinets. Ultimately, we must invest in efforts to endow the vast amount of current 3D assets with motion, where our work is only a starting point. With that effort, we also must deal with the “missing interior” problem as few, if any, current 3D models contain interior structures.

REFERENCES

Ben Abbatematteo, Stefanie Tellex, and George Konidaris. 2019. Learning to generalize kinematic models to novel objects. In *Proceedings of the 3rd Conference on Robot Learning*.

Amirhossein Alimohammadi, Sauradip Nag, Saeid Asgari Taghanaki, Andrea Tagliasachi, Ghassan Hamarneh, and Ali Mahdavi Amiri. 2024. SMITE: Segment Me In TimE. *arXiv preprint arXiv:2410.18538* (2024).

Yogesh Balaji, Seungjung Nah, Xun Huang, Arash Vahdat, Jiaming Song, Karsten Kreis, Miika Aittala, Timo Aila, Samuli Laine, Bryan Catanzaro, et al. 2022. ediffi: Text-to-image diffusion models with an ensemble of expert denoisers. *arXiv preprint arXiv:2211.01324* (2022).

Andreas Blattmann, Tim Dockhorn, Sumith Kulal, Daniel Mendelevitch, Maciej Kilian, Dominik Lorenz, Yam Levi, Zion English, Vikram Voleti, Adam Letts, et al. 2023a. Stable video diffusion: Scaling latent video diffusion models to large datasets. *arXiv preprint arXiv:2311.15127* (2023).

Andreas Blattmann, Robin Rombach, Huan Ling, Tim Dockhorn, Seung Wook Kim, Sanja Fidler, and Karsten Kreis. 2023b. Align your latents: High-resolution video synthesis with latent diffusion models. In *Proceedings of the IEEE/CVF Conference on Computer Vision and Pattern Recognition*. 22563–22575.

Angel X Chang, Thomas Funkhouser, Leonidas Guibas, Pat Hanrahan, Qixing Huang, Zimo Li, Silvia Savarese, Manolis Savva, Shuran Song, Hao Su, Jianxiong Xiao, Li Yi, and Fisher Yu. 2015. ShapeNet: An information-rich 3D model repository. *arXiv preprint arXiv:1512.03012* (2015).

Jasmine Collins, Shubham Goel, Kenan Deng, Achleshwar Luthra, Leon Xu, Erhan Gundogdu, Xi Zhang, Tomas F Yago Vicente, Thomas Dideriksen, Himanshu Arora, Matthieu Guillaumin, and Jitendra Malik. 2022. ABO: Dataset and benchmarks for real-world 3D object understanding. In *CVPR*. 21126–21136.

Yuren Cong, Mengmeng Xu, Christian Simon, Shoufa Chen, Jiawei Ren, Yanping Xie, Juan-Manuel Perez-Rua, Bodo Rosenhahn, Tao Xiang, and Sen He. 2024. FLAT-TEN: optical FLOW-guided ATTENTION for consistent text-to-video editing. (2024). *arXiv:2310.05922 [cs.CV]* <https://arxiv.org/abs/2310.05922>

Matt Deitke, Ruoshi Liu, Matthew Wallingford, Huong Ngo, Oscar Michel, Aditya Kusupati, Alan Fan, Christian LaForte, Vikram Voleti, Samir Yitzhak Gadre, et al. 2024. Objaverse-xl: A universe of 10M+ 3d objects. *Advances in Neural Information Processing Systems* 36 (2024).

Matt Deitke, Ruoshi Liu, Matthew Wallingford, Huong Ngo, Oscar Michel, Aditya Kusupati, Alan Fan, Christian LaForte, Vikram Voleti, Samir Yitzhak Gadre, Eli VanderBilt, Aniruddha Kembhavi, Carl Vondrick, Georgia Gkioxari, Kiana Ehsani, Ludwig Schmidt, and Ali Farhadi. 2023. Objaverse-XL: A Universe of 10M+ 3D Objects. *arXiv:2307.05663 [cs.CV]* <https://arxiv.org/abs/2307.05663>

Huan Fu, Rongfei Jia, Lin Gao, Mingming Gong, Binqiang Zhao, Steve Maybank, and Dacheng Tao. 2021. 3d-future: 3d furniture shape with texture. *International Journal of Computer Vision* 129 (2021), 3313–3337.

Songwei Ge, Ceyuan Yang, Anyi Rao, Zhengyang Liang, Yaohui Wang, Yu Qiao, Maneesh Agrawala, Dahu Lin, and Bo Dai. 2023. Animatediff: Animate your personalized text-to-image diffusion models without specific tuning. *arXiv preprint arXiv:2307.04725* (2023).

Jonathan Ho, William Chan, Chitwan Saharia, Jay Whang, Ruiqi Gao, Alexey Gritsenko, Diederik P. Kingma, Ben Poole, Mohammad Norouzi, David J. Fleet, and Tim Salimans. 2022. Imagen Video: High Definition Video Generation with Diffusion Models. *arXiv:2210.02303 [cs.CV]* <https://arxiv.org/abs/2210.02303>

Jonathan Ho, Ajay Jain, and Pieter Abbeel. 2020. Denoising diffusion probabilistic models. *Advances in neural information processing systems* 33 (2020), 6840–6851.

Ruizhen Hu, Wenchao Li, Oliver Van Kaick, Ariel Shamir, Hao Zhang, and Hui Huang. 2017. Learning to predict part mobility from a single static snapshot. *ACM Transactions On Graphics (TOG)* 36, 6 (2017), 1–13.

Denys Iliash, Hanxiao Jiang, Yiming Zhang, Manolis Savva, and Angel X Chang. 2024. S2O: Static to openable enhancement for articulated 3D objects. *arXiv preprint arXiv:2409.18896* (2024).

Ajinkya Jain, Rudolf Lioutikov, Caleb Chuck, and Scott Niekum. 2021. Screwnet: Category-independent articulation model estimation from depth images using screw theory. In *2021 IEEE International Conference on Robotics and Automation (ICRA)*. IEEE, 13670–13677.

Hyeonho Jeong, Geon Yeong Park, and Jong Chul Ye. 2023. VMC: Video Motion Customization using Temporal Attention Adaption for Text-to-Video Diffusion Models. *arXiv preprint arXiv:2312.00845* (2023).

Hanxiao Jiang, Yongsen Mao, Manolis Savva, and Angel X Chang. 2022. OPD: Single-view 3D openable part detection. In *European Conference on Computer Vision*. Springer, 410–426.

Yanqin Jiang, Li Zhang, Jin Gao, Weimin Hu, and Yao Yao. 2023. Consistent4d: Consistent 360 $\{\deg\}$ dynamic object generation from monocular video. *arXiv preprint arXiv:2311.02848* (2023).

Mukul Khanna, Yongsen Mao, Hanxiao Jiang, Sanjay Haresh, Brennan Shacklett, Dhruv Batra, Alexander Clegg, Eric Undersander, Angel X Chang, and Manolis Savva. 2024. Habitat synthetic scenes dataset (hssd-200): An analysis of 3d scene scale and realism tradeoffs for objectgoal navigation. In *Proceedings of the IEEE/CVF Conference on Computer Vision and Pattern Recognition*. 16384–16393.

Diederik P Kingma and Jimmy Ba. 2014. Adam: A method for stochastic optimization. *arXiv preprint arXiv:1412.6980* (2014).

Diederik P Kingma and Max Welling. 2013a. Auto-encoding variational bayes. *arXiv preprint arXiv:1312.6114* (2013).

Diederik P Kingma and Max Welling. 2013b. Auto-encoding variational bayes. *arXiv preprint arXiv:1312.6114* (2013).

Long Le, Jason Xie, William Liang, Hung-Ju Wang, Yue Yang, Yecheng Jason Ma, Kyle Vedder, Arjun Krishna, Dinesh Jayaraman, and Eric Eaton. 2024. Articulate-Anything: Automatic Modeling of Articulated Objects via a Vision-Language Foundation Model. *arXiv preprint arXiv:2410.13882* (2024).

Guillaume Le Moing, Jean Ponce, and Cordelia Schmid. 2021. CCVS: context-aware controllable video synthesis. *Advances in Neural Information Processing Systems* 34 (2021), 14042–14055.

Jiahui Lei, Congyu Deng, William B Shen, Leonidas J Guibas, and Kostas Daniilidis. 2023. Nap: Neural 3d articulated object prior. *Advances in Neural Information Processing Systems* 36 (2023), 31878–31894.

Ruining Li, Chuanxia Zheng, Christian Rupprecht, and Andrea Vedaldi. 2024. Puppetmaster: Scaling interactive video generation as a motion prior for part-level dynamics. *arXiv preprint arXiv:2408.04631* (2024).

Jiayi Liu, Denys Iliash, Angel X Chang, Manolis Savva, and Ali Mahdavi-Amiri. 2024a. SINGAPO: Single Image Controlled Generation of Articulated Parts in Object. *arXiv preprint arXiv:2410.16499* (2024).

Jiayi Liu, Ali Mahdavi-Amiri, and Manolis Savva. 2023a. Paris: Part-level reconstruction and motion analysis for articulated objects. In *Proceedings of the IEEE/CVF International Conference on Computer Vision*. 352–363.

Jiayi Liu, Hou In Ivan Tam, Ali Mahdavi-Amiri, and Manolis Savva. 2024b. CAGE: Controllable Articulation GEneration. In *Proceedings of the IEEE/CVF Conference on Computer Vision and Pattern Recognition*. 17880–17889.

Ruoshi Liu, Rundi Wu, Basile Van Hoorick, Pavel Tokmakov, Sergey Zakharov, and Carl Vondrick. 2023b. Zero-1-to-3: Zero-shot One Image to 3D Object. *arXiv:2303.11328 [cs.CV]*

Zhengxiong Luo, Dayou Chen, Yingya Zhang, Yan Huang, Liang Wang, Yujun Shen, Deli Zhao, Jingren Zhou, and Tieniu Tan. 2023. VideoFusion: Decomposed Diffusion Models for High-Quality Video Generation. In *Proceedings of the IEEE/CVF Conference on Computer Vision and Pattern Recognition*. 10209–10218.

Joanna Materzynska, Josef Sivic, Eli Shechtman, Antonio Torralba, Richard Zhang, and Bryan Russell. 2023. Customizing motion in text-to-video diffusion models. *arXiv preprint arXiv:2312.04966* (2023).

Gal Metzer, Elad Richardson, Or Patashnik, Raja Giryes, and Daniel Cohen-Or. 2023. Latent-nerf for shape-guided generation of 3d shapes and textures. In *Proceedings of the IEEE/CVF Conference on Computer Vision and Pattern Recognition*. 12663–12673.

Ben Mildenhall, Pratul P Srinivasan, Matthew Tancik, Jonathan T Barron, Ravi Ramamoorthi, and Ren Ng. 2021. Nerf: Representing scenes as neural radiance fields for view synthesis. *Commun. ACM* 65, 1 (2021), 99–106.

Alexander H. Miller, Will Feng, Dhruba Tirumala, Adam Fisch, Augustus Odena, Vivek Ramavajjalai, Joel Z. Leibo, Kelvin Guu and Jesse Engel, Jack Clark, Maruan H. Ali, Nazneen Rajani, Iain J. Dunning, Jacob Andreas, Chris Dyer, Dario Amodei, Jakob Uszkoreit, Douwe Piekstra, Tom Brown, and Ilya Sutskever. 2020. CLIP: Learning to Solve Visual Tasks by Unsupervised Learning of Language Representations. In *International Conference on Machine Learning*.

Kaichun Mo, Leonidas J Guibas, Mustafa Mukadam, Abhinav Gupta, and Shubham Tulsiani. 2021. Where2act: From pixels to actions for articulated 3d objects. In *Proceedings of the IEEE/CVF International Conference on Computer Vision*. 6813–6823.

Kaichun Mo, Shilin Zhu, Angel X. Chang, Li Yi, Subarna Tripathi, Leonidas J. Guibas, and Hao Su. 2019. PartNet: A Large-Scale Benchmark for Fine-Grained and Hierarchical Part-Level 3D Object Understanding. In *The IEEE Conference on Computer Vision and Pattern Recognition (CVPR)*.

Eyal Molad, Eliahu Horwitz, Dani Vavelski, Alex Rav Acha, Yossi Matias, Yael Pritch, Yaniv Leviathan, and Yedid Hoshen. 2023. Dreamix: Video Diffusion Models are General Video Editors. *arXiv preprint arXiv:2302.01329* (2023).

Sauradip Nag, Xiatian Zhu, Jiankang Deng, Yi-Zhe Song, and Tao Xiang. 2023. Diff4d: Temporal action detection with proposal denoising diffusion. In *Proceedings of the IEEE/CVF International Conference on Computer Vision*. 10362–10374.

Adam Paszke, Sam Gross, Francisco Massa, Adam Lerer, James Bradbury, Gregory Chanan, Trevor Killeen, Zeming Lin, Natalia Gimelshein, Luca Antiga, et al. 2019. Pytorch: An imperative style, high-performance deep learning library. *Advances in neural information processing systems* 32 (2019).

Ethan Perez, Florian Strub, Harm De Vries, Vincent Dumoulin, and Aaron Courville. 2018. Film: Visual reasoning with a general conditioning layer. In *Proceedings of the AAAI conference on artificial intelligence*, Vol. 32.

Ben Poole, Ajay Jain, Jonathan T. Barron, and Ben Mildenhall. 2022. DreamFusion: Text-to-3D using 2D Diffusion. *arXiv* (2022).

Aditya Ramesh, Mikhail Pavlov, Gabriel Goh, Scott Gray, Chelsea Voss, Alec Radford, Mark Chen, and Ilya Sutskever. 2021. Zero-shot text-to-image generation. In *International Conference on Machine Learning*. PMLR, 8821–8831.

Nikhila Ravi, Jeremy Reizenstein, David Novotny, Taylor Gordon, Wan-Yen Lo, Justin Johnson, and Georgia Gkioxari. 2020. Accelerating 3d deep learning with pytorch3d. *arXiv preprint arXiv:2007.08501* (2020).

Jiawei Ren, Liang Pan, Jiaxiang Tang, Chi Zhang, Ang Cao, Gang Zeng, and Ziwei Liu. 2023. Dreamgaussian4d: Generative 4d gaussian splatting. *arXiv preprint arXiv:2312.17142* (2023).

Robin Rombach, Andreas Blattmann, Dominik Lorenz, Patrick Esser, and Björn Ommer. 2022a. High-resolution image synthesis with latent diffusion models. In *Proceedings of the IEEE/CVF Conference on Computer Vision and Pattern Recognition*. 10684–10695.

Robin Rombach, Andreas Blattmann, Dominik Lorenz, Patrick Esser, and Björn Ommer. 2022b. High-resolution image synthesis with latent diffusion models. In *Proceedings of the IEEE/CVF conference on computer vision and pattern recognition*. 10684–10695.

Olaf Ronneberger, Philipp Fischer, and Thomas Brox. 2015. U-net: Convolutional networks for biomedical image segmentation. In *Medical image computing and computer-assisted intervention—MICCAI 2015: 18th international conference, Munich, Germany, October 5–9, 2015, proceedings, part III* 18. Springer, 234–241.

Yichun Shi, Peng Wang, Jianglong Ye, Mai Long, Kejie Li, and Xiao Yang. 2023. Mvdream: Multi-view diffusion for 3d generation. *arXiv preprint arXiv:2308.16512* (2023).

Uriel Singer, Adam Polyak, Thomas Hayes, Xi Yin, Jie An, Songyang Zhang, Qiyuan Hu, Harry Yang, Oron Ashual, Oran Gafni, et al. 2022a. Make-a-video: Text-to-video generation without text-video data. *arXiv preprint arXiv:2209.14792* (2022).

Uriel Singer, Adam Polyak, Thomas Hayes, Xi Yin, Jie An, Songyang Zhang, Qiyuan Hu, Harry Yang, Oron Ashual, Oran Gafni, et al. 2022b. Make-a-video: Text-to-video generation without text-video data. *arXiv preprint arXiv:2209.14792* (2022).

Uriel Singer, Shelly Sheynin, Adam Polyak, Oron Ashual, Iurii Makarov, Filippos Kokkinos, Naman Goyal, Andrea Vedaldi, Devi Parikh, Justin Johnson, et al. 2023. Text-to-4d dynamic scene generation. *arXiv preprint arXiv:2301.11280* (2023).

Jascha Sohl-Dickstein, Eric Weiss, Niru Maheswaranathan, and Surya Ganguli. 2015. Deep unsupervised learning using nonequilibrium thermodynamics. In *International conference on machine learning*. PMLR, 2256–2265.

Jiaming Song, Chenlin Meng, and Stefano Ermon. 2020a. Denoising diffusion implicit models. *arXiv preprint arXiv:2010.02502* (2020).

Yang Song and Stefano Ermon. 2019. Generative modeling by estimating gradients of the data distribution. *Advances in neural information processing systems* 32 (2019).

Yang Song, Jascha Sohl-Dickstein, Diederik P Kingma, Abhishek Kumar, Stefano Ermon, and Ben Poole. 2020b. Score-based generative modeling through stochastic differential equations. *arXiv preprint arXiv:2011.13456* (2020).

Jiaxiang Tang. 2022. Stable-dreamfusion: Text-to-3D with Stable-diffusion. <https://github.com/ashawkey/stable-dreamfusion>.

Thomas Unterthiner, Sjoerd van Steenkiste, Karol Kurach, Raphaël Marinier, Marcin Michalski, and Sylvain Gelly. 2019. FVD: A new metric for video generation. (2019).

Lukas Uzolas, Elmar Eisemann, and Petr Kellnhofer. 2024. MotionDreamer: Zero-Shot 3D Mesh Animation from Video Diffusion Models. *arXiv preprint arXiv:2405.20155* (2024).

Patrick von Platen, Suraj Patil, Anton Lozhkov, Pedro Cuenca, Nathan Lambert, Kashif Rasul, Mishig Davaadorj, Dhruv Nair, Sayak Paul, William Berman, Yiyi Xu, Steven Liu, and Thomas Wolf. 2022. Diffusers: State-of-the-art diffusion models. <https://github.com/huggingface/diffusers>.

Jiuniu Wang, Hangjie Yuan, Dayou Chen, Yingya Zhang, Xiang Wang, and Shiwei Zhang. 2023. Modelscope text-to-video technical report. *arXiv preprint arXiv:2308.06571* (2023).

Peng Wang and Yichun Shi. 2023. Imagedream: Image-prompt multi-view diffusion for 3d generation. *arXiv preprint arXiv:2312.02201* (2023).

Xiang Wang, Hangjie Yuan, Shiwei Zhang, Dayou Chen, Jiuniu Wang, Yingya Zhang, Yujun Shen, Deli Zhao, and Jingren Zhou. 2024b. Videocomposer: Compositional video synthesis with motion controllability. In *NeurIPS*, Vol. 36.

Xiaogang Wang, Bin Zhou, Yahao Shi, Xiaowu Chen, Qimping Zhao, and Kai Xu. 2019. Shape2motion: Joint analysis of motion parts and attributes from 3d shapes. In *Proceedings of the IEEE/CVF Conference on Computer Vision and Pattern Recognition*. 8876–8884.

Zhengyi Wang, Cheng Lu, Yikai Wang, Fan Bao, Chongxuan Li, Hang Su, and Jun Zhu. 2024a. Prolificdreamer: High-fidelity and diverse text-to-3d generation with variational score distillation. *Advances in Neural Information Processing Systems* 36 (2024).

Fangyu Wei, Rohan Chabra, Lingni Ma, Christoph Lassner, Michael Zollhoefer, Szymon Rusinkiewicz, Chris Sweeney, Richard Newcombe, and Mira Slavcheva. 2022. Self-supervised Neural Articulated Shape and Appearance Models. In *Proceedings IEEE/CVF Conference on Computer Vision and Pattern Recognition (CVPR)*.

Jay Zhangjie Wu, Yixiao Ge, Xintao Wang, Stan Weixian Lei, Yuchao Gu, Wynne Hsu, Ying Shan, Xiaohu Qie, and Mike Zheng Shou. 2022. Tune-A-Video: One-Shot Tuning of Image Diffusion Models for Text-to-Video Generation. *arXiv preprint arXiv:2212.11565* (2022).

Ruiqi Wu, Liangyu Chen, Tong Yang, Chunle Guo, Chongyi Li, and Xiangyu Zhang. 2023. Lamp: Learn a motion pattern for few-shot-based video generation. *arXiv preprint arXiv:2310.10769* (2023).

Fanbo Xiang, Yuzhe Qin, Kaichun Mo, Yikuan Xia, Hao Zhu, Fangchen Liu, Minghua Liu, Hanxiao Jiang, Yifei Yuan, He Wang, et al. 2020. Sapien: A simulated part-based interactive environment. In *Proceedings of the IEEE/CVF conference on computer vision and pattern recognition*. 11097–11107.

Jinbo Xing, Menghan Xia, Yong Zhang, Haoxin Chen, Wangbo Yu, Hanyuan Liu, Gongye Liu, Xintao Wang, Ying Shan, and Tien-Tsin Wong. 2024. Dynamicroft: Animating open-domain images with video diffusion priors. In *European Conference on Computer Vision*. Springer, 399–417.

Ling Yang, Zhilong Zhang, Yang Song, Shenda Hong, Runsheng Xu, Yue Zhao, Wentao Zhang, Bin Cui, and Ming-Hsuan Yang. 2023. Diffusion models: A comprehensive survey of methods and applications. *Comput. Surveys* 56, 4 (2023), 1–39.

Lijun Yu, Yong Cheng, Kihyuk Sohn, José Lezama, Han Zhang, Huiwen Chang, Alexander G Hauptmann, Ming-Hsuan Yang, Yuan Hao, Irfan Essa, et al. 2023a. Magvit: Masked generative video transformer. In *Proceedings of the IEEE/CVF Conference on Computer Vision and Pattern Recognition*. 10459–10469.

Xin Yu, Yuan-Chen Guo, Yangguang Li, Ding Liang, Song-Hai Zhang, and Xiaojuan Qi. 2023b. Text-to-3d with classifier score distillation. *arXiv preprint arXiv:2310.19415* (2023).

Richard Zhang, Phillip Isola, Alexei A Efros, Eli Shechtman, and Oliver Wang. 2018. The Unreasonable Effectiveness of Deep Features as a Perceptual Metric. In *CVPR*.

Rui Zhao, Yuchao Gu, Jay Zhangjie Wu, David Junhao Zhang, Jia-Wei Liu, Weijia Wu, Jussi Keppo, and Mike Zheng Shou. 2024. Motiondirector: Motion customization of text-to-video diffusion models. In *European Conference on Computer Vision*. Springer, 273–290.

Yufeng Zheng, Xueteng Li, Koki Nagano, Sifei Liu, Otmar Hilliges, and Shalini De Mello. 2024. A unified approach for text-and image-guided 4d scene generation. In *Proceedings of the IEEE/CVF Conference on Computer Vision and Pattern Recognition*. 7300–7309.

Daquan Zhou, Weimin Wang, Hanshu Yan, Weiwei Lv, Yizhe Zhu, and Jiashi Feng. 2022. Magicvideo: Efficient video generation with latent diffusion models. *arXiv preprint arXiv:2211.11018* (2022).

A ALGORITHM

Here, we explain in detail the algorithm used to retrieve the motion axis and origin from the point cloud. In this paper, we consider two types of motion, 1) Revolute Motion 2) Prismatic Motion.

Revolute Motion. Given a set of vertices of a mesh \mathcal{M} the revolute motion is represented as:

$$\vec{x}^* = \mathbf{R}(\vec{x} - \vec{o}) + \vec{o} \quad (13)$$

where, \vec{x} is the original mesh vertex, \vec{x}^* is the transformed mesh vertex after articulation, \vec{o} is motion axis origin, \mathbf{R} is the rotation matrix around the predicted motion axis direction, $\vec{a} = [a_x, a_y, a_z]$. Here, $\|\vec{a}\| = 1$. Given an angle θ , with which we want to rotate around the motion axis, we can compute the rotation matrix using Rodrigues formula as,

$$\mathbf{K} = \begin{bmatrix} 0 & -a_z & a_y \\ a_z & 0 & -a_x \\ -a_y & a_x & 0 \end{bmatrix}, \quad (14)$$

$$\mathbf{R} = \mathbf{I} + \sin(\theta) \mathbf{K} + (1 - \cos(\theta)) \mathbf{K}^2 \quad (15)$$

Prismatic Motion. Unlike revolute motion, prismatic motion is defined using only motion axis, \vec{a} , where $\|\vec{a}\| = 1$. Given a motion range $[M_{max}, M_{min}]$ within which we would like to articulate a part, the magnitude γ and ultimately the transformed vertex of the mesh \mathcal{M} is defined as:

$$\vec{a}^* = \gamma * \vec{a}, \quad \vec{x}^* = \vec{x} + \vec{a}^* \quad (16)$$

where, γ is the magnitude of scaling computed from the motion range, \vec{x} is the original mesh vertex and \vec{x}^* is the transformed mesh vertex. The algorithm to find motion parameters is described in Algorithm 1.

B ADDITIONAL RESULTS

We present additional results on PartNet Sapien Dataset [Xiang et al. 2020]. The results are shown in Fig. 10. The part to be articulated is highlighted. As can be seen in the figure, our model is able to generalize within the same category of object of PartNet Sapien Dataset. In addition to this, we also show additional results of the generalization capability of our model on ACD dataset [Iliash et al. 2024] i.e. the diffusion model is trained on PartNet Sapien dataset and tested on ACD dataset for generalization. As can be seen in Fig. 11 and Fig. 12 can generalize to unseen shapes over a different dataset. We also show articulation results on the 3D mesh in the last column.

ALGORITHM 1: Find_Motion_Parameters()

```

input : Static Mesh  $\mathcal{M}$ , Point Clouds  $P_{N_f}$ , Motion Type  $M_{type}$ ,  

    Segmentation Labels  $L$ , Instance ID  $y$ 
output: Motion Axis  $\vec{a}$ , Motion Origin  $\vec{o}$ 
 $\vec{a}, \vec{o} \leftarrow \vec{0}, \vec{0}$ ;
// Find OBB, where  $OB = (\vec{v}_1, \vec{v}_2, \vec{v}_3, \vec{c}, d_{v_1}, d_{v_2}, d_{v_3})$ 
 $OOB \leftarrow \text{Find_Oriented_Bounding_Box}(\mathcal{M}, y)$  ;
 $A_{hyp} \leftarrow (\vec{v}_1, \vec{v}_2, \vec{v}_3, -\vec{v}_1, -\vec{v}_2, -\vec{v}_3)$ ;
 $O_{hyp} \leftarrow (\vec{c} \pm 0.5(d_{v_1} \cdot \vec{v}_1), \vec{c} \pm 0.5(d_{v_2} \cdot \vec{v}_2), \vec{c} \pm 0.5(d_{v_3} \cdot \vec{v}_3), \vec{c})$ ;
 $min\_dist \leftarrow 0.0$ ;
for each  $\vec{a}_i$  in  $A_{hyp}$  do
    for each  $\vec{o}_i$  in  $O_{hyp}$  do
        // transform vertices of  $\mathcal{M}$  as per  $M_{type}$  & find best match.
        if  $M_{type} = \text{"revolute"}$  then
            | Mesh  $\mathcal{M}' \leftarrow \text{Revolute}(\mathcal{M}, \vec{a}_i, \vec{o}_i, y)$  // Eq: 13
        end
        if  $M_{type} = \text{"prismatic"}$  then
            | Mesh  $\mathcal{M}' \leftarrow \text{Prismatic}(\mathcal{M}, \vec{a}_i, y)$  // Eq: 16
        end
         $P_{\mathcal{M}} \leftarrow \mathcal{M}.\text{vertices}$ ;
         $e \leftarrow \text{chamfer\_distance}(P_{\mathcal{M}}, P_{N_f})$ ;
        if  $e < min\_dist$  then
            |  $\vec{a} \leftarrow \vec{a}_i$ ;  $\vec{o} \leftarrow \vec{o}_i$ 
        end
    end
end

```



Fig. 10. Qualitative results of Multi-View Video Generation on PartNet Sapian Dataset.



Fig. 11. Qualitative results of generalization of Multi-view video generation and articulation estimation on ACD dataset [Iliash et al. 2024].

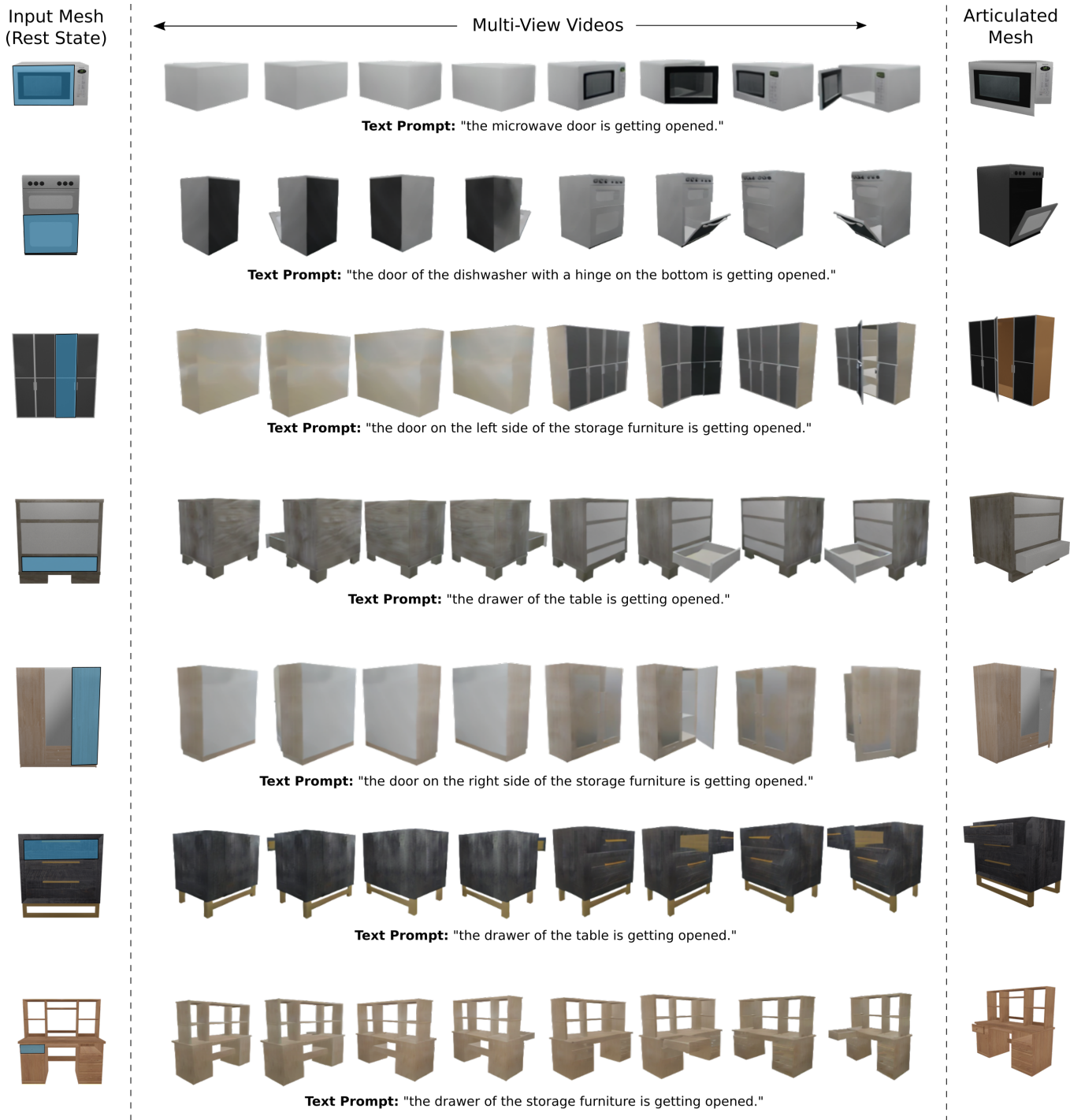


Fig. 12. Qualitative results of generalization of Multi-view video generation and articulation estimation on ACD dataset [Iliash et al. 2024].